Extending the potential of plasma-induced luminescence spectroscopy

Elise Clavé, Michael Gaft, Vincent Motto-Ros, Cécile Fabre, Olivier Forni, Olivier Beyssac, Sylvestre Maurice, Roger Wiens, Bruno Bousquet

Extending the potential of plasma-induced luminescence spectroscopy

Elise Clavé[1], Michael Gaft[2], Vincent Motto-Ros[3], Cécile Fabre[4], Olivier Forni[5], Olivier Beyssac[6], Sylvestre Maurice[5], Roger C. Wiens[7], Bruno Bousquet[1]

[1] CELIA, UMR CNRS 5107, Université de Bordeaux, 351 Cours de la Libération, F-33405 Talence Cedex, France
[2] Ariel University, Physical Department, Ariel, Israel
[3] Institut Lumière Matière, Université Lyon 1, CNRS, 69622 Villeurbanne, France
[4] GeoRessources UMR CNRS 7359, Université de Lorraine, F-54500 Vandoeuvre, France
[5] Institut de Recherche en Astrophysique et Planétologie, CNRS/Université de Toulouse, UPS-OMP, Toulouse France
[6] Institut de Minéralogie, de Physique des Matériaux et de Cosmochimie (IMPMC), UMR 7590 Sorbonne Université, CNRS & MNHN, Campus Jussieu, CC115 4 place Jussieu, 75005 Paris, France
[7] Los Alamos National Laboratory, Los Alamos, NM, USA

corresponding author: elise.clave@u-bordeaux.fr

Abstract

In the context of laser-induced breakdown spectroscopy (LIBS), plasma-induced luminescence (PIL) may be observed by tuning the temporal acquisition parameters (delay and gate). This approach provides useful information about minor elements in a sample. The broad range of excitation resulting from the laser-induced plasma enables the simultaneous observation of multiple luminescence emission bands. However, PIL results in damage to the sample due to laser ablation. Moreover, time resolution only enables the separation of emission signatures with different decay times; as a consequence, only luminescence signatures with long decay times may be observed separately from plasma emissions. In this study, we propose a new experimental approach to extend the potential of PIL spectroscopy. Our main idea is to generate a laser-induced plasma on a separate ablation target adjacent to the luminescent sample, which is hence protected from laser ablation. Moreover, the ablation target can be selected to ensure a stable plasma for PIL excitation. We also show that this setup enables the further study of the excitation mechanisms of PIL itself by varying the nature of the excitation source of PIL. Finally, we propose a new experimental setup that enables the study of the luminescence features of short decay times. We successfully tested this new approach on both artificial and natural crystals, showing luminescence emission bands of varying decay times.

1. Introduction

Plasma-induced luminescence (PIL) is the name given to the phenomenon of luminescence emission after excitation by a plasma. To the best of our knowledge, it was first studied in the context of cold plasma treatment [1,2]. Polymer samples were irradiated for 5 to 180 s by a plasma induced by electrical discharge, and their resulting luminescence was studied as a function of plasma exposure time. PIL was later associated with laser spectroscopy and laser-induced plasmas by Gaft *et al.* [3]. In the context of laser-induced breakdown spectroscopy (LIBS), a pulsed laser of high energy (millijoule range) is focused at the surface of a sample. The laser fluence is thus sufficient to ablate, vaporize and excite a small amount of matter, resulting in the formation of a plasma composed of the chemical elements present in the sample and the ambient gas in neutral and ionized excited states. When the plasma cools down, radiative relaxation processes occur, producing the atomic and ionic emission lines that compose the LIBS spectrum, providing access to the elemental composition of the sample [4]. Practically, the LIBS spectrum varies over the lifetime of the plasma. In the first ~100 ns, the plasma temperature is typically 15,000 K or more, and the electron density is typically $10^{17} cm^{-3}$ or more [5]. This results in an emission spectrum dominated by a continuum due to Bremsstrahlung and recombination radiation, which is usually considered background of LIBS measurements. Then, emission from ions typically decays in 100 to 500 ns for the multi-ionized species [6] and several µs for singly ionized species. Emission lines from neutral atoms can be detected for up to 10 µs, and finally, molecular emission bands resulting from recombination within the plasma can be observed in some cases during a few tens of microseconds. Time-resolved LIBS thus gives access to information of different natures. Indeed, tuning the delay after the laser pulse as well as the gate, namely, the duration of acquisition, allows somewhat specific observation of either ionic, neutral or molecular spectral features in LIBS spectra and the extraction of complementary data. The acquisition parameters (delay and gate) are generally optimized to improve the signal-to-noise ratio and the contrast between continuum and atomic lines and to reduce spectral broadening effects [7]. Their control also enables accurate studies of molecular emissions [8,9]. For instance, the detection and quantification of fluorine in geological samples has been demonstrated through the study of CaF emission bands [10,11]. Moreover, in several cases, plasma-induced luminescence can also be detected [3,12], making PIL an additional signal accessible with a time-resolved LIBS experimental setup simply by tuning the delay and gate parameters of the acquisition. Previous studies have shown that the observation of PIL, in addition to LIBS information, improves the detection capabilities for minor elements [13–15]. In some cases, such as for rare earth elements, the detection capability of PIL may even reach the ppb level [14]. Luminescence relies on emissions from impurities and defects within the lattice of a material [12,16], and the broad variety of plasma emissions provides different possible excitation sources for luminescence. PIL thus appears to be a type of spectroscopy with great potential and a high complementarity with LIBS studies and can be easily implemented using classic LIBS experimental setups.

However, PIL presents several difficulties. First, as with LIBS, it relies upon laser ablation of the studied material. This results in local damage to the sample: target erosion appears in the form of an ablation crater [17]. Moreover, Fau *et al.* observed that LIBS laser shots could result in local amorphization, melting and/or phase transformation in the sample [18]. PIL is therefore a locally destructive technique, whereas rare or precious samples require fully nondestructive analyses. Moreover, recording a PIL spectrum with a satisfying signal-to-noise ratio generally requires accumulation of the signal over a significant number of laser shots (for example, in [14], the PIL signal is collected over 1000 shots). However, these experimental conditions are not compatible with the analysis of fragile samples likely to be destroyed during the acquisition of spectra, thus preventing

one from obtaining a decent PIL spectrum under these conditions. Finally, due to the colocation (both spatial and spectral) of plasma emission and luminescence, efficient separation of these two signals relies upon the selection of appropriate time windows [3,14] when luminescence emission bands exhibit longer decay times than the emission lines related to plasma radiation. Therefore, luminescence signatures related to short decay times may be hidden by the more intense LIBS emission lines and hardly observed in the PIL spectra.

An alternative setup, called *in-air PIL*, was proposed by Veltri *et al.* [19] and relies on laser-plasma electron acceleration to perform cathodoluminescence measurements in atmospheric conditions. By using the interaction of a focused femtosecond laser with air, the authors created an in-air plasma located a few millimeters from the sample, in which PIL excitation occurred and was observed. In addition to the advantages mentioned by the authors, this approach also prevents any damage to the samples, allowing a decent PIL signal to be obtained, even on fragile samples. Even though in-air laser-induced plasma can be achieved by nanosecond laser interactions [20], the related papers [19,21] only mention the use of femtosecond lasers for luminescence excitation.

Similar to pulsed-laser deposition [22], in which the laser-induced plasma is created on a solid target located close to the substrate to be treated, we propose for the first time to examine the advantage of performing PIL spectroscopy with a laser-induced plasma expanding in ambient air after nanosecond laser pulse interactions occur on a separate ablation target near the luminescent sample. In this case, the sample probed by PIL is not damaged, and the excitation spectrum can be tuned by selecting different ablation targets or using optical filters, which is naturally an extension to the case of in-air plasma discussed above. Furthermore, we demonstrate in the last part of our study that separating the plasma from the luminescent sample allows additional optical filtering as a unique solution to separate short decay time luminescence bands from plasma emission lines. Finally, it is worth pointing out that this paper is not dealing with the advantages of PIL compared to other luminescence techniques , but claims to describe possible extensions of the PIL technique itself.

2. Standard PIL experiment

We first introduce in this section the standard PIL experimental setup and results that we will consider as the reference for further discussion. Our experimental setup is schematically displayed in Fig. 1. It corresponds to a classic LIBS setup. It consists of a diode-pumped pulsed Nd:YAG laser (Viron, Lumibird) delivering 1064 nm – 6 ns – 10 Hz pulses. The laser fluence onto the sample surface is approximately 50 J/cm², and the spot diameter is approximately 200 micrometers. The laser beam is vertically focused through a 10-cm fused silica plano-convex lens onto the surface of the crystal sample. The PIL radiation is collected and then injected into a circle-to-linear bundle of 19 optical fibers (each fiber is 2-m long and has a 100-µm core diameter) by a 5-cm converging lens and finally introduced into a Czerny-Turner spectrometer (Kymera 328i, Andor) equipped with a 1200 l/mm grating blazed at 300 nm. An intensified CCD camera (iStar CCD 340, Andor) enables the tuning of the delay and gate parameters, as well as the gain, for signal amplification.

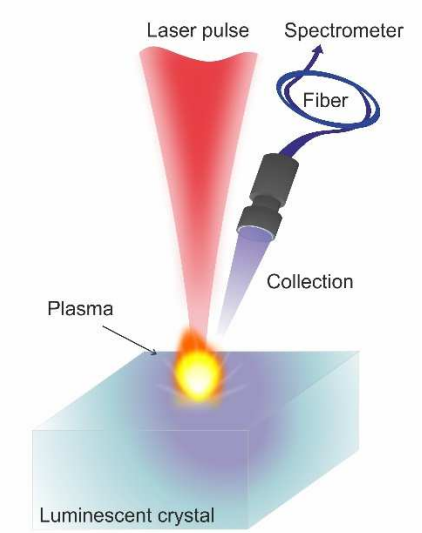

Figure 1 - Scheme of our PIL experimental setup

The luminescent sample is a 6x6x12 mm sapphire crystal (Al_2O_3) doped with titanium, hereafter referred to as Ti:Sa. This crystal was selected as a case study since it contains three luminescing ions, Ti^{3+}, and Ti^{4+}, as expected, and Cr^{3+} as an impurity. These three ions exhibit well known and relatively intense emission features with significantly different decay times. More precisely, Ti^{3+} exhibits a broad emission band between 650 and 900 nm, with a decay time on the microsecond time scale, while the luminescence signature of Ti^{4+} is a band at approximately 410 nm that lasts several tens of microseconds. Finally, Cr^{3+} is characterized by a doublet of emission lines at approximately 693 nm that decays in several milliseconds [23]. Fig. 2 shows two PIL spectra of this Ti:Sa crystal recorded with two different time windows to consider the microsecond and millisecond range decay times. More precisely, Fig. 2a corresponds to a delay of 50 µs and a gate of 10 ms, while Fig. 2b displays a spectrum recorded with a delay of 2 µs and a gate of 30 µs. Note that these spectra and all the spectra presented in this paper are not corrected for the instrument response function; they are only corrected for the background signal. The PIL spectrum displayed in Fig. 2a exhibits the emission features related to Ti^{4+} and Cr^{3+}, free from any plasma radiation due to the relatively long delay (i.e., 50 µs). Fig. 2b shows the luminescence band of Ti^{3+}, as well as some plasma atomic emission lines. According to the NIST database [24], these lines correspond to the Al II line at 624.34 nm, the H-α line at 656.28 nm and the Al I doublet at 669.61 and 669.87 nm. The lines at approximately 616 and 618 nm probably correspond to the second order of the Al I doublet at 308.21 and 309.28 nm. Fig. 2b illustrates the fact that LIBS and PIL spectral features may overlap when the luminescence decay time is relatively short, namely, in the microsecond range or below.

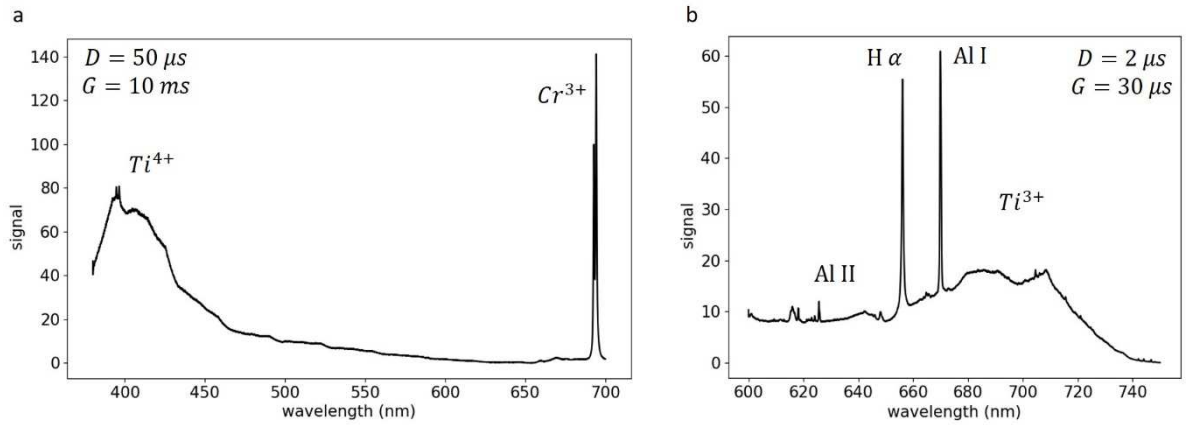

Figure 2 – PIL spectrum of a Ti:Sa crystal: (a) Ti^{4+} and Cr^{3+} luminescence signatures acquired with a delay of $50\ \mu s$, gate of $10\ ms$, and gain of 3000 using 500 accumulations (b) Ti^{3+} luminescence signature and plasma emission lines acquired with a delay of $2\ \mu s$, gate of $30\ \mu s$ and gain of 2000 by using 100 accumulations.

Standard PIL is based on laser ablation and plasma creation at the sample surface. In some cases, it cannot be implemented, and it is necessary to turn to modified PIL configurations to keep the sample safe.

3. *Side PIL* configuration

3.1. PIL signal excited by an adjacent plasma

We propose a new experimental approach in which laser-induced plasma is not generated at the surface of the sample itself but at the surface of a target adjacent to the luminescent crystal, as illustrated in Fig. 3. In this way, the sample of interest is not damaged by laser ablation. Moreover, the ablation target can be chosen to ensure that a stable plasma can be sustained at its surface, over hundreds of laser shots, to provide stable excitation for PIL in the adjacent sample. Third, in this configuration, one can insert an optical filter between the plasma and luminescent crystal to select the energy range of the plasma photons used for PIL excitation.

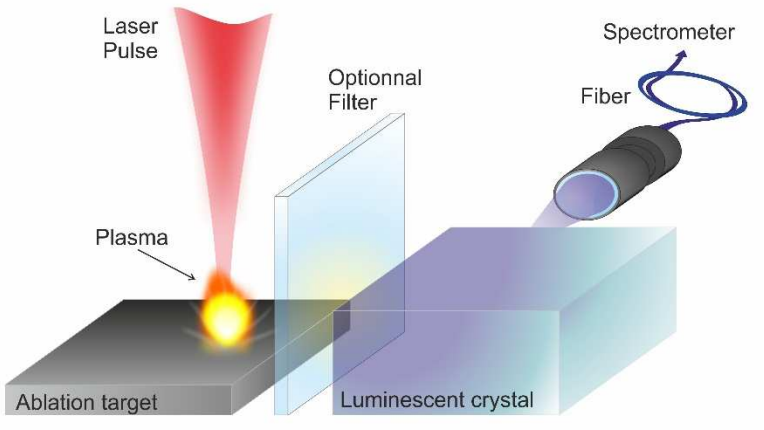

Figure 3 – Scheme of a *side-PIL* experiment with an optional optical filter used to filter out part of the excitation spectrum.

We conducted a series of *side PIL* experiments on the Ti:Sa crystal already presented in the case of standard PIL measurements in Section 2. We use a piece of steel as the ablation target. The distance between the plasma and the entrance face of the Ti:Sa crystal is approximately 7 mm, and the entrance face is unpolished. We use a longpass filter with an edge at 300 nm. Thus, when the filter is inserted in the light path, only excitation photons from the plasma at wavelengths above 300 nm

reach the crystal. Fig. 4 shows the PIL spectra obtained in this configuration, with and without the optical filter. The time parameters are the same as those used in regular PIL in the previous section.

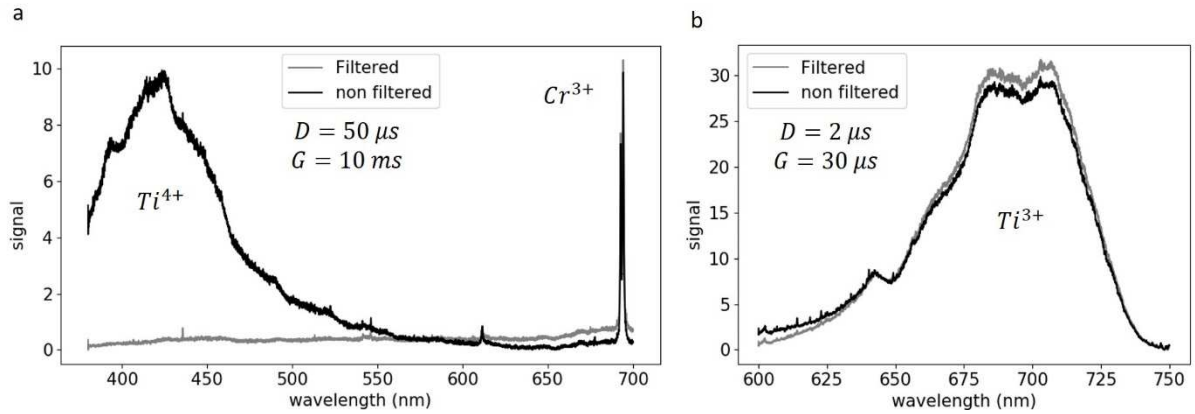

Figure 4 – *Side-PIL* spectra (after dark removal) of the Ti:Sa crystal obtained from a steel plasma without (black curves) and with (gray) an optical filter. In this case, the distance between the plasma and entrance face of the crystal was approximately 7 mm, and the entrance face of the crystal was unpolished. The optical filter used here transmits only radiation with wavelengths above 300 nm. (a) Ti^{4+} and Cr^{3+} luminescence signatures acquired with a delay of 50 µs, gate of 10 ms and gain of 4000 by using 500 accumulations; (b) Ti^{3+} luminescence signature acquired with a delay of 2 µs, gate of 30 µs and gain of 4000 by using 500 accumulations.

First, we can see in Fig. 4 that without a filter (black curve), the same luminescence signatures are observed in *side PIL*, as were observed in regular PIL in Fig. 2 (a. Ti^{4+} and Cr^{3+} with a long delay, and b. Ti^{3+} with a short delay). This shows that laser ablation does not have to take place directly on the luminescent sample for PIL to be observed. Moreover, the Cr^{3+} and Ti^{3+} signatures are mostly unaffected by the addition of the filter between the plasma and Ti:Sa crystal. Based on the filter's transmission characteristics, these bands are excited by photons above 300 nm. This is consistent with the fact that Alombert-Goget *et al.* reported that these bands are excited between 350 and 600 nm [23]. The small differences observed in these signatures may be explained by the interaction of the plasma light with the optical filter itself, namely, the existence of a luminescence signal induced within the filter in the spectral range from 400 to 750 nm [25,26]. In the case of our experimental data, this luminescence from the optical filter, which has its own temporal characteristics, may explain why the intensity observed at wavelengths greater than 600 nm can increase with using the filter. One can note that atomic emission lines from the laser-induced plasma of Ti:Sa were visible in Fig. 2b, whereas no atomic emission line is clearly observed in Fig. 4b, despite the time parameters being similar between the two experiments. This is probably because in *side PIL*, observation is not directly oriented towards the plasma. However, we also observed during other tests that plasma emission lines were detected under the experimental conditions corresponding to those of Fig. 4b when the light from the plasma entered the sample through a polished face (as opposed to what is obtained for an unpolished face, as shown in Fig. 4b) of the same crystal. The amount of residual excitation lines in the PIL spectra is probably due to propagation conditions supported by reflection, refraction and scattering at the entrance face of the crystal, but this is beyond the scope of the present study, although it may be worth investigating further.

Concerning the Ti^{4+} emission band, however, we can see that the introduction of the filter results in the complete disappearance of this band, indicating that its excitation source is blocked by the filter. Since the filter has a transmission close to zero for photons with wavelengths less than 300 nm, this is consistent with the known excitation band of Ti^{4+} in photoluminescence, which is between 200 and 270 nm [23].

Luminescence excitation observed in *side PIL* is therefore totally consistent with photonic excitation occurring simultaneously in the UV and visible ranges. Moreover, tuning the spectral range of the

plasma radiation reaching the luminescent sample enables us to observe different emission bands independently and to understand the excitation process responsible for each emission band. This is the first extension of the classic PIL configuration.

3.2. Influence of the ablation target on the PIL spectrum

Side PIL also offers new opportunities to investigate how excitation spectra from different ablation targets affect the luminescence spectrum of a given sample. This study requires recording i) the emission spectra of the ablation plasmas obtained on different targets and ii) the PIL spectra resulting from each plasma. In particular, it allows us to understand how the material-specific radiation of the plasma, i.e., the atomic, ionic and molecular emission lines observed in LIBS, contributes to the total radiation emitted by the plasma and, therefore, how it affects the PIL spectra.

Since the excitation of the Ti^{3+} and Cr^{3+} bands occur between 350 and 600 nm, as reported in [23], we decided to record and compare the plasma emission spectra of three ablation targets in this spectral range, as well as the corresponding *side PIL* spectra.

We use the same Ti:Sa crystal used in the tests described in the previous sections. The ablation targets are pieces of steel (same as that described in Section 3.1), aluminum and copper with flat surfaces that are large enough for pristine ablation locations to be used for each new round of measurements. For each metallic target, the laser-induced plasma was kept at the same height and distance (approximately 7 mm) relative to the entrance face of the Ti:Sa crystal sample. We do not use a filter here. The LIBS and *side PIL* spectra are shown in Fig. 5.

a

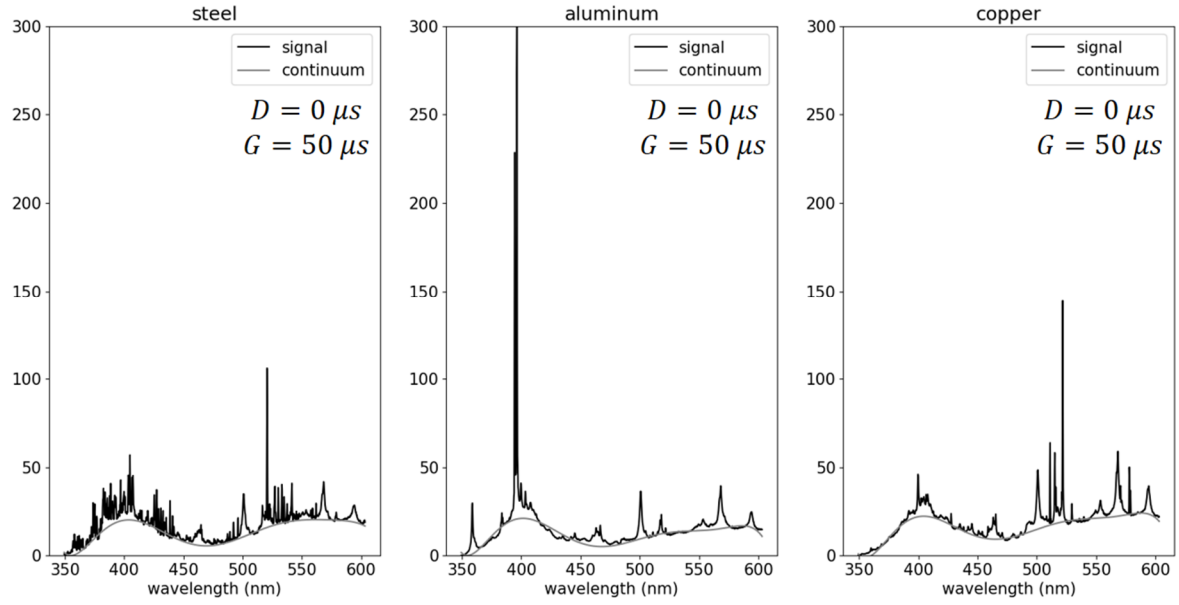

b c

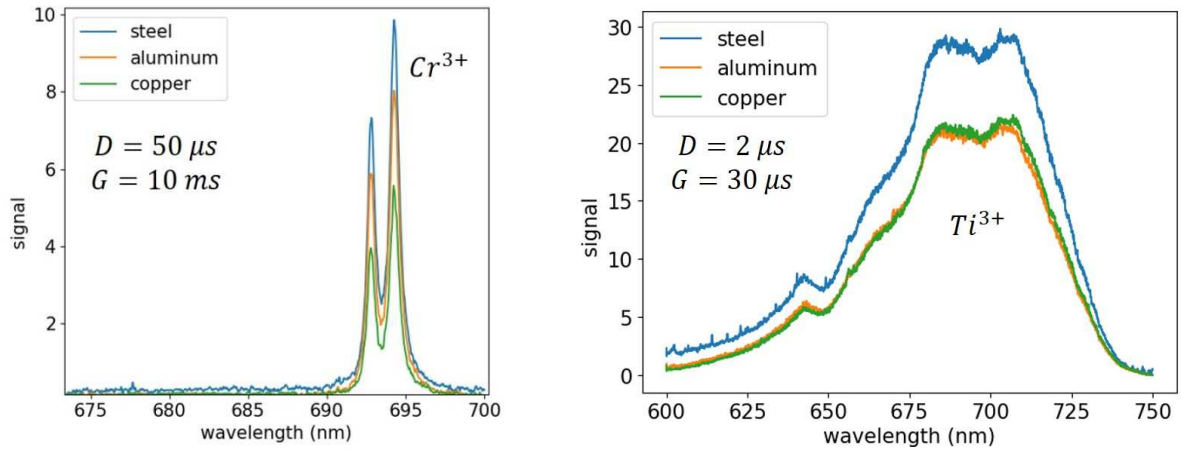

Figure 5 – (a) Plasma radiation (time-integrated LIBS) spectra obtained for the three ablation targets (black), steel, aluminum, and copper, right after the laser pulse (delay of 0) and with a gate of $50\ \mu s$. Polynomial fitting curves (degree of 7) displayed in gray are given as a rough estimate of the baseline (continuum). (b-c) Close magnified view of the *side PIL* spectra of the Ti:Sa crystal excited by the plasma radiation of steel (blue), aluminum (orange) and copper (green), exhibiting (b) the Cr^{3+} band with a delay of $50\ \mu s$ and gate of $10\ ms$ and (c) the Ti^{3+} band with a delay of $2\ \mu s$ and gate of $30\ \mu s$, both of which were obtained with a gain of 4000 by using 500 accumulations for each ablation target.

Let us consider the spectra of the plasma radiation obtained on the three ablation targets, as shown in Fig. 5a. We set the delay to 0 and the gate to $50\ \mu s$ to ensure that the total plasma radiation is recorded for each ablation target, including the continuum, atomic emission lines, and molecular bands, with varying relative weights as the plasma expands and cools down. The continuum is mainly related to the physical conditions of ablation, followed by plasma formation and expansion, whereas atomic lines and molecular bands depend on the chemical composition of the ablation target. To roughly estimate the relative contribution of the continuum to the total plasma radiation, the continuum was fitted with a polynomial function of degree 7. From Fig. 5a, one can directly observe that all three polynomial fits (gray curves) are quite similar both in shape and in intensity. On the other hand, the atomic, ionic and molecular spectral signatures greatly differ from one spectrum to the other. Indeed, the LIBS spectrum of the steel target exhibits a large series of emission lines between 350 and 550 nm related to iron, while for the aluminum target, the spectrum is dominated by the very intense Al I doublet at 394.40-396.15 nm and then by significantly weaker AlO molecular emission bands due to recombination processes occurring in air. For the copper target, several Cu I lines can be seen, especially between 500 and 600 nm, as well as molecular bands with much lower intensities than the atomic emission lines. We computed the ratio of the area under the fitted curve of the continuum to the total area under the LIBS spectrum in the spectral range of 350-600 nm. This ratio ranges between 76 and 82% depending on the ablation target. Even if this rough estimate does not consider the instrument response function, one can reasonably conclude that between 350 and 600 nm, the plasma radiation is dominated by continuum emission. We observed in Fig. 5a that the continuum emission does not vary much from one plasma to the next. Consequently, the plasma radiation, in the visible range, at the origin of the *side PIL* is dominated by the continuum's contribution, which is independent of the choice of the ablation target. Finally, note that the plasma spectra displayed in Fig. 5a should also be corrected by the absorption probability at each wavelength to obtain the actual contribution of each wavelength to luminescence excitation if one wants to accurately interpret the differences in intensity observed in the PIL spectra.

Considering the *side-PIL* spectra shown in Fig. 5b-c, it appears that the Cr^{3+} and Ti^{3+} signatures are excited by plasma radiation from the three targets. For the Cr^{3+} doublet emission, the largest intensity is observed for the steel target, followed by aluminum and copper, and the intensities vary by a factor of up to 2. For the Ti^{3+} signature, copper and aluminum targets induce very similar emission intensities, while the steel target induces a slight increase in intensity (less than 1.5 higher).

The other spectral feature we examine is the Ti^{4+} luminescence band, which is known to be excited between 225 and 250 nm [23]. The *side PIL* Ti^{4+} signatures induced using our three ablation targets are shown in Fig. 6. We observe that the signal intensity is five times higher with the steel plasma, compared to the other two ablation targets. This indicates a significant difference in intensity between the plasma radiations of steel on the one hand, and aluminum and copper on the other hand, in the spectral range 225-250 nm. This conclusion is in good agreement with the simulated LIBS spectra derived from the NIST database [24], that show a very large number of highly emissive lines from the iron contained in steel. Aluminum and copper exhibit far fewer lines in this spectral range. This could also be verified by an appropriate experimental setup.

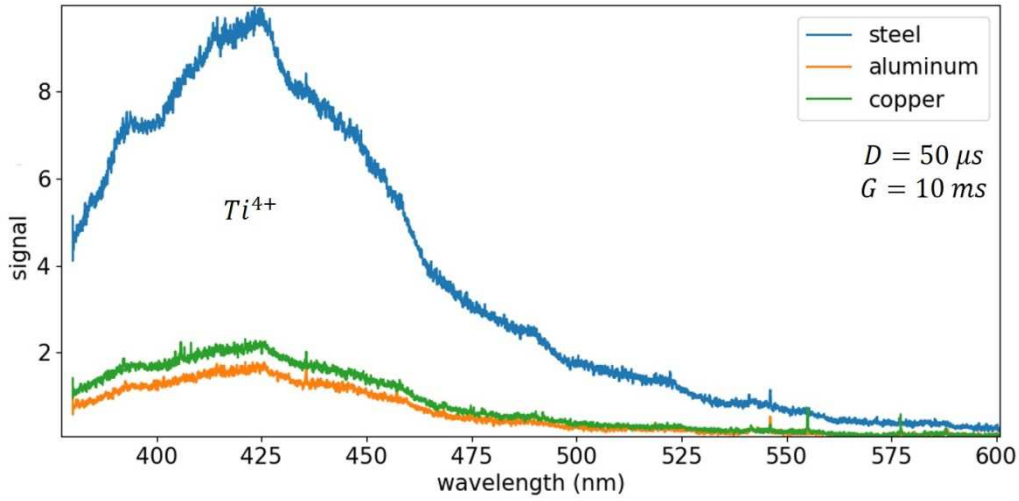

Figure 6 – Side PIL spectra of Ti:Sa crystal excited by radiation in the UV range from the plasma created after the laser ablation of steel (blue), aluminum (orange) and copper (green). In this case, the distance between the plasma and entrance face of the crystal was approximately 7 mm, and the entrance face of the crystal was unpolished. The Ti^{4+} luminescence signature was acquired with a delay of 50 µs, gate of 10 ms and gain of 4000 by using 500 accumulations.

We can conclude that in *side PIL*, luminescence excitation occurs due to the photons emitted by the ablation plasma over the whole spectral range simultaneously. The use of an optical filter placed between the plasma and luminescent sample enables tuning of the spectral range used for PIL excitation. We compared the PIL excitation resulting from ablation plasmas obtained on three different targets and concluded that in the visible range, the continuum is both predominant and similar for all plasmas, resulting in similar PIL emission spectra. For luminescence signatures excited in the UV range, the differences observed when changing the ablation target are in good agreement with the simulated spectra of plasma emission but were out of the spectral range accessible with our experimental setup. Based on this study, we concluded that the choice of the ablation target to initiate PIL is not critical, and we decided to use only the plasma induced on the steel ablation target for further experiments.

Finally, thanks to the *side PIL* configuration proposed here, it is possible to record luminescence spectra after excitation by plasma radiation without damaging the sample by laser ablation and using only classic LIBS equipment. However, the proximity between the crystal and plasma, which is required to optimize the excitation, exposes the crystal to the risk of vapor or particle deposition, resulting in a surface coating forming on the crystal, as observed in pulsed laser deposition, which may not be acceptable for precious samples or samples that require further analysis.

4. *Remote PIL* configuration

4.1. First demonstration on a Ti:Sa crystal

To protect the sample from coating by plasma ejection, we propose in this section another experimental setup, which we call *remote PIL*. In *remote PIL*, the plasma volume is imaged inside the luminescent sample thanks to a standard imaging system consisting of two converging lenses, as illustrated in Fig. 7. The laser-induced plasma is thus located at the focal point of the first lens, the collected light propagates as a collimated beam, and the second lens focuses the beam inside the luminescent sample. Under such conditions, any optional optical filter can easily be introduced between the two lenses, and the luminescent sample can be placed several tens of centimeters away from the plasma, which prevents any risk of deposition. In our case, the focal distance of the two UV-fused silica plano-convex converging lenses was 5 cm, and the plasma-sample distance was close to 20 cm. The choice of the material used for the converging lenses is critical since its UV cutoff determines the highest energy of the photons eventually available for luminescence excitation in *remote PIL*, and, therefore, the emission bands that can be observed.

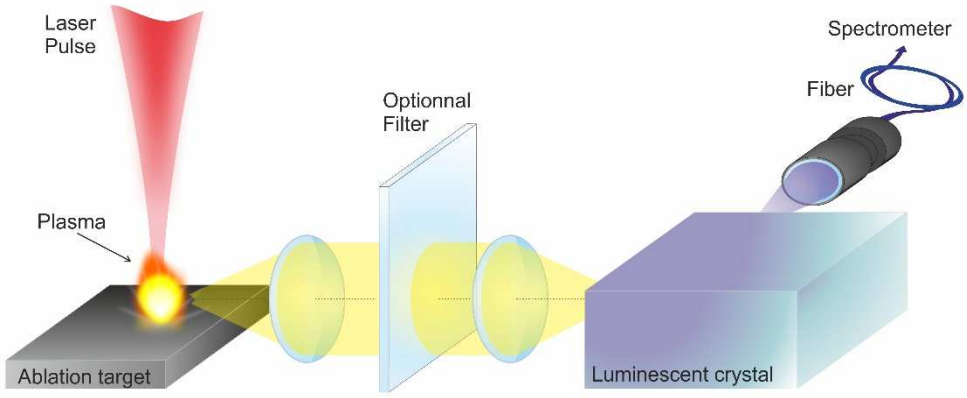

Figure 7 – Scheme of the experimental setup used for *remote PIL*

To demonstrate the ability of this new experimental setup to perform PIL measurements, we implemented the experimental setup of *remote PIL* described in Fig. 7 for the case of using a steel sample as the ablation target and Ti:Sa crystal as the luminescent sample. The PIL spectrum of Ti:Sa recorded in this configuration, with the same acquisition parameters as those selected to obtain the *side PIL* spectra presented in Fig. 4, is displayed in Fig. 8. However, smoothing (with a moving average over 21 pixels) was applied to these spectra to reduce noise since the intensity of the *remote PIL* signal recorded under these experimental conditions was quite low.

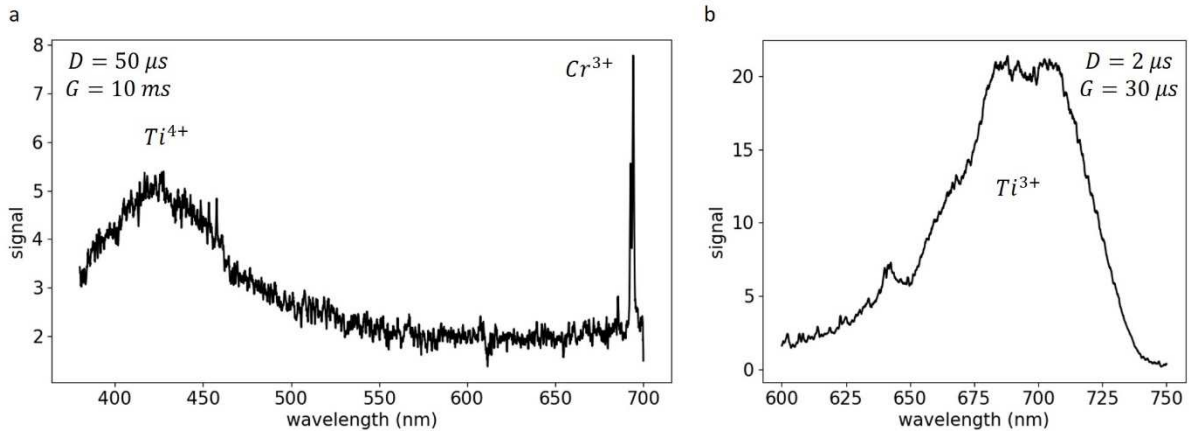

Figure 8 – *Remote PIL* spectrum of the Ti:Sa crystal obtained after laser ablation of a steel target; (a) Ti^{4+} and Cr^{3+} luminescence signatures acquired with a delay of $50\ \mu s$, gate of $10\ ms$ and gain of 4000 by using 500 accumulations; (b)

Ti^{3+} luminescence signature acquired with a delay of 2 μs, gate of 30 μs and gain of 4000 by using 500 accumulations. The spectra were processed in the following way: the dark spectrum was subtracted, and a moving average over 21 pixels was applied.

From Fig. 8, one can conclude that *remote PIL* has been successfully demonstrated in the case of the selected Ti:Sa sample located more than 20 cm away from the plasma to avoid any risk of damage.

4.2. Application to a natural crystal of apatite

Subsequently, to demonstrate that *remote PIL* is not limited to the characterization of highly luminescent synthesized crystals, we replaced the Ti:Sa crystal with a natural sample of Durango apatite ($Ca_5(PO_4)_3(OH,Cl,F)$). This sample is well known for its enrichment in rare earth elements, which exhibit well-known luminescence bands [12]. In this practical case, we failed to acquire a satisfying PIL spectrum under the standard PIL conditions, namely, by forming the plasma on the surface of the sample itself. In fact, this sample is too fragile to sustain several hundred laser shots at a given location, the material is ablated very quickly, and the plasma is not stable enough to enable luminescence observation with a sufficiently good signal-to-noise ratio. The *remote PIL* spectrum of this sample is displayed in Fig. 9.

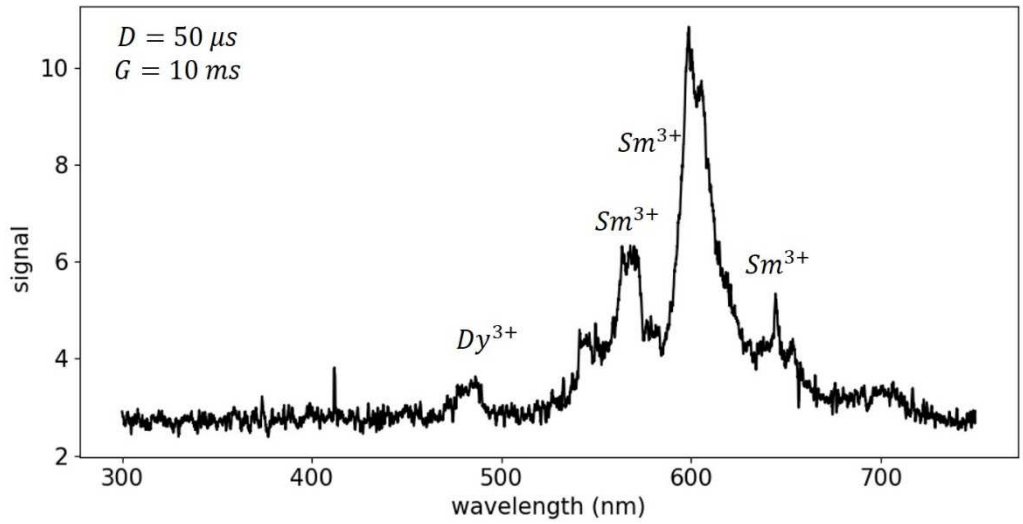

Figure 9 – *Remote PIL* spectrum of Durango apatite obtained with a delay of 50 μs, a gate of 10 ms, a gain of 4000 and 500 accumulations. Sm^{3+} signatures are visible at approximately 570, 600 and 645 nm. Dy^{3+} is observed at 480 nm. The spectrum was processed in the following way: the dark spectrum was subtracted, and a moving average over 21 pixels was applied.

From Fig. 9, several spectral signatures related to rare-earth elements present in this apatite sample can be easily identified, and more precisely, some lines/bands related to Sm^{3+} and Dy^{3+} are observed [12]. This result demonstrates that the new setup we have proposed to record PIL spectra remotely can also be applied to the characterization of natural samples and emphasizes the advantage of this nondestructive method in the case of fragile samples.

4.3. Application to short-lived luminescence

The other advantage of *remote PIL* is that it provides the ability to perform optical filtering of excitation light. In the standard PIL configuration, the time delay and gate are specifically adjusted to filter out the atomic emission lines and molecular recombination bands from the plasma and record the luminescence spectral features in the best conditions of the signal-to-noise ratio. However, in some cases, there are luminescence features that exhibit fast decay times, namely, less than 1 µs,

and thus, the temporal filtering commonly applied in PIL is not sufficient in such cases to separate the sample luminescence and the plasma emission lines, which exhibit the same decay time. This is still the case for *remote PIL* but we demonstrate that additional optical filtering makes it possible to overcome this problem. To this end, we selected an artificial fluorite crystal activated by Eu^{2+}. The emission band of Eu^{2+}, peaking at approximately 425 nm, is known to decay in less than $1\ \mu s$ [27]. The *remote PIL* spectrum of this sample recorded with a delay of 0 and a gate of 5 µs is displayed in Fig. 10.

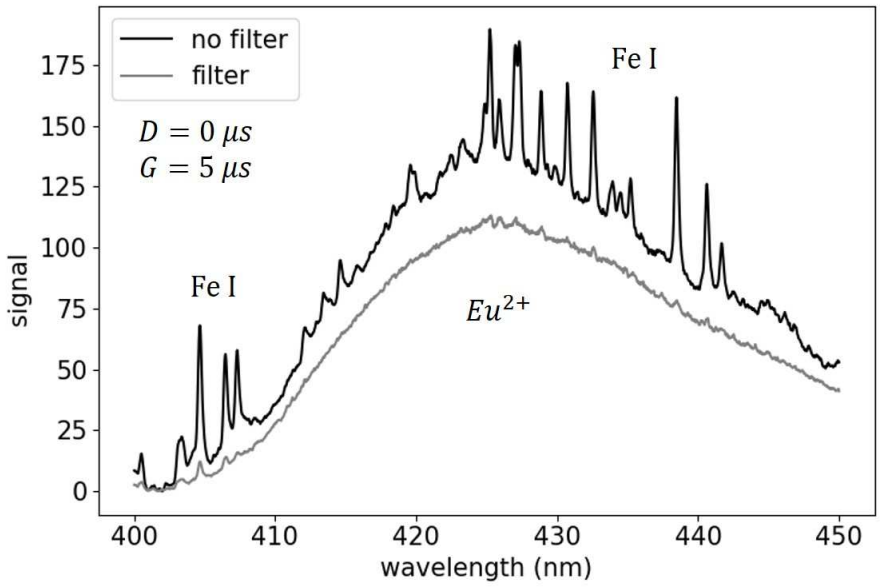

Figure 10 – *Remote PIL* spectrum of Eu^{2+}:CaF_2 obtained immediately after the laser pulse (delay of 0) with a gate of 5 μs and without an optical filter (black line), showing LIBS emission lines from light transmitted into the crystal, and that with an optical filter (gray line) after correction by the transmittance value of the filter, in which only Eu^{2+} luminescence remains.

Fig. 10 shows a *remote PIL* spectrum of Eu^{2+}:CaF_2 composed of Eu^{2+} luminescence band (400-450 nm) and the atomic emission lines (from iron in this case) from the ablation target (steel in this case). We now introduce an optical filter into the light path of the excitation radiation coming from the plasma. The filter is characterized by a transmittance value close to 50% in the 300-360 nm range and close to 0% in the 400-650 nm range. With this filter (gray curve), the plasma emission is drastically attenuated in the spectral range presented in Fig. 10, making it possible to retrieve from the PIL spectrum only luminescence signatures, without any additional contribution. Note that the spectra presented in Fig. 10 could also have been recorded under the s*ide PIL* conditions. However, the optical filter would have been potentially damaged due to its proximity to the laser-induced plasma. Finally, this example of a fluorite sample emphasizes the advantage of the *remote PIL* configuration to analyze fast decaying emission bands that the temporal resolution cannot separate from the plasma emission lines.

More generally, the selection of optional optical filters, which one can introduce in the light path of the *remote PIL* setup, could allow us to significantly extend the potential of PIL. Indeed, while the luminescence excited without a filter is the result of excitation by a broadband plasma radiation spectrum, optical filters could allow us to tailor this spectrum to specifically excite selected transitions. Thus, *remote PIL* may offer new opportunities for luminescence excitation, midway between classical PIL, in which all wavelengths simultaneously contribute to excitation, and classic photoluminescence, in which a single selected wavelength induces luminescence excitation at one time.

Conclusion

We describe two new experimental setups easily made with classic LIBS equipment, and we discuss their ability to achieve PIL measurements. For these two configurations, the plasma is not created on the sample surface but is instead made at the surface of a target dedicated to laser ablation and plasma formation. The *side PIL* configuration was first implemented to demonstrate that separating plasma formation from luminescence was viable for spectroscopy. This setup also allowed us to demonstrate that plasma photons over the whole spectral range contribute to PIL excitation. The demonstration was achieved by using a Ti:Sa crystal as the luminescent sample and three different ablation targets, namely, steel, aluminum and copper. The comparison of the PIL spectra obtained with the three plasmas, as well as the study of the plasma emissions detected over the first $50\ \mu s$ after the laser pulse, shows that PIL excitation in the visible range is dominated by the continuum of the plasma emission. The result of UV excitation on PIL was consistent with the simulated LIBS spectra but was not experimentally verified. In the second experimental setup, *remote PIL*, the plasma is created on the ablation target and is directed into the luminescent crystal, located several tens of centimeters away. This setup allowed us to insert an optical filter between the imaging lenses and thus filter out the atomic emission lines from plasma radiation that overlap with the short decay time luminescence emission bands. We validated this setup by using Ti:Sa again, as well as a natural Durango apatite sample and an artificial crystal of fluorite enriched in Eu^{2+}, which is known to decay in less than $1\ \mu s$. We believe this new approach may enable various new laboratory studies on plasma-induced luminescence.

Acknowledgments

We thank Inka Manek-Hönninger (CELIA, Univ. Bordeaux, France) for providing us with the Ti:Sa crystal and Gediminas Janusauskas (LOMA, Univ. Bordeaux, France) for lending us the optical filter used to observe the Eu^{2+} signature in fluorite with *remote PIL*.

Funding: This work was supported by CNES and Region Nouvelle Aquitaine.

References

[1] G. Teyssedre, P. Tiemblo, F. Massines, C. Laurent, On the UV contribution to plasma-induced luminescence of polypropylene, J. Phys. D: Appl. Phys. 29 (1996) 3137–3146. https://doi.org/10.1088/0022-3727/29/12/031.

[2] F. Massines, P. Tiemblo, G. Teyssedre, C. Laurent, On the nature of the luminescence emitted by a polypropylene film after interaction with a cold plasma at low temperature, Journal of Applied Physics. 81 (1997) 937–943. https://doi.org/10.1063/1.364186.

[3] M. Gaft, L. Nagli, Y. Groisman, Plasma induced luminescence (PIL), Optical Materials. 34 (2011) 368–375. https://doi.org/10.1016/j.optmat.2011.05.024.

[4] R. Noll, Laser-Induced Breakdown Spectroscopy, Springer Berlin Heidelberg, Berlin, Heidelberg, 2012. https://doi.org/10.1007/978-3-642-20668-9.

[5] A.D. Giacomo, Laser-induced plasma emission: from atomic to molecular spectra, Appl. Phys. (2017) 18.

[6] M. Gaft, L. Nagli, I. Gornushkin, Y. Groisman, Doubly ionized ion emission in laser-induced breakdown spectroscopy in air, Anal Bioanal Chem. 400 (2011) 3229–3237. https://doi.org/10.1007/s00216-011-4847-0.

[7] R. Fantoni, L. Caneve, F. Colao, L. Fornarini, V. Lazic, V. Spizzichino, Laser Induced Breakdown Spectroscopy (LIBS), Advances in Spectroscopy f or Lasers and Sensing. (2006) 229–254. https://doi.org/10.1007/1-4020-4789-4_13.

[8] C.G. Parigger, Atomic and molecular emissions in laser-induced breakdown spectroscopy, Spectrochimica Acta Part B: Atomic Spectroscopy. 79–80 (2013) 4–16. https://doi.org/10.1016/j.sab.2012.11.012.
[9] D.S. Vogt, K. Rammelkamp, S. Schröder, H.W. Hübers, Molecular emission in laser-induced breakdown spectroscopy: An investigation of its suitability for chlorine quantification on Mars, Icarus. 302 (2018) 470–482. https://doi.org/10.1016/j.icarus.2017.12.006.
[10] O. Forni, M. Gaft, M.J. Toplis, S.M. Clegg, S. Maurice, R.C. Wiens, N. Mangold, O. Gasnault, V. Sautter, S.L. Mouélic, P.-Y. Meslin, M. Nachon, R.E. McInroy, A.M. Ollila, A. Cousin, J.C. Bridges, N.L. Lanza, M.D. Dyar, First detection of fluorine on Mars: Implications for Gale Crater's geochemistry, Geophysical Research Letters. 42 (2015) 1020–1028. https://doi.org/10.1002/2014GL062742.
[11] M. Gaft, L. Nagli, N. Eliezer, Y. Groisman, O. Forni, Elemental analysis of halogens using molecular emission by laser-induced breakdown spectroscopy in air, Spectrochimica Acta Part B: Atomic Spectroscopy. 98 (2014) 39–47. https://doi.org/10.1016/j.sab.2014.05.011.
[12] M. Gaft, R. Reisfeld, G. Panczer, Modern Luminescence Spectroscopy of minerals and materials, 2015.
[13] L. Liu, S. Li, X. Huang, Y. Lu, K. Chen, R. Pik, L. Jiang, J.F. Silvain, Y.F. Lu, Detection of trace-level uranium and samarium in glasses by combined laser-induced breakdown spectroscopy and plasma-induced fluorescence spectroscopy, J. Anal. At. Spectrom. 30 (2015) 1128–1132. https://doi.org/10.1039/C5JA00020C.
[14] M. Gaft, Y. Raichlin, F. Pelascini, G. Panzer, V. Motto Ros, Imaging rare-earth elements in minerals by laser-induced plasma spectroscopy: Molecular emission and plasma-induced luminescence, Spectrochimica Acta Part B: Atomic Spectroscopy. 151 (2019) 12–19. https://doi.org/10.1016/j.sab.2018.11.003.
[15] M. Gaft, L. Nagli, I. Gornushkin, Y. Raichlin, Laser-induced breakdown spectroscopy of BaF_2-Tm^{3+}, Spectrochimica Acta Part B: Atomic Spectroscopy. 164 (2020) 105767. https://doi.org/10.1016/j.sab.2020.105767.
[16] C. Ronda, Luminescence - From Theory to Applications, Wiley-VCH, Weinheim, 2008.
[17] V.N. Rai, S.N. Thakur, Physics of Plasma in Laser-Induced Breakdown Spectroscopy, in: Laser-Induced Breakdown Spectroscopy, Elsevier, 2007: pp. 83–111. https://doi.org/10.1016/B978-044451734-0.50007-7.
[18] A. Fau, O. Beyssac, M. Gauthier, P.Y. Meslin, A. Cousin, K. Benzerara, S. Bernard, J.C. Boulliard, O. Gasnault, O. Forni, R.C. Wiens, M. Morand, P. Rosier, Y. Garino, S. Pont, S. Maurice, Pulsed laser-induced heating of mineral phases: Implications for laser-induced breakdown spectroscopy combined with Raman spectroscopy, Spectrochimica Acta Part B: Atomic Spectroscopy. 160 (2019) 105687. https://doi.org/10.1016/j.sab.2019.105687.
[19] S. Veltri, M. Barberio, C. Liberatore, M. Scisciò, A. Laramée, L. Palumbo, F. Legaré, P. Antici, Laser stimulated plasma-induced luminescence for on-air material analysis, Appl. Phys. Lett. 110 (2017) 021114. https://doi.org/10.1063/1.4973467.
[20] K. Dzierżęga, A. Mendys, S. Pellerin, E. Thouin, G. Travaille, B. Bousquet, L. Canioni, B. Pokrzywka, Thomson scattering from laser induced plasma in air, J. Phys.: Conf. Ser. 227 (2010) 012029. https://doi.org/10.1088/1742-6596/227/1/012029.
[21] M. Barberio, E. Skantzakis, P. Antici, Material analysis using laser-plasma driven luminescence spectroscopy, Journal of Luminescence. 214 (2019) 116603. https://doi.org/10.1016/j.jlumin.2019.116603.
[22] D.P. Norton, Pulsed Laser Deposition of Complex Materials: Progress Toward Applications, in: Pulsed Laser Deposition of Thin Films, John Wiley & Sons, Ltd, 2006: pp. 1–31. https://doi.org/10.1002/9780470052129.ch1.
[23] G. Alombert-Goget, H. Li, Y. Guyot, A. Brenier, K. Lebbou, Luminescence and coloration of undoped and Ti-doped sapphire crystals grown by Czochralski technique, Journal of Luminescence. 169 (2016) 516–519. https://doi.org/10.1016/j.jlumin.2015.02.001.

[24] NIST LIBS Database, (n.d.). https://physics.nist.gov/PhysRefData/ASD/LIBS/libs-form.html (accessed October 27, 2020).
[25] J. Fournier, J. Neauport, P. Grua, E. Fargin, V. Jubera, D. Talaga, S. Jouannigot, Green luminescence in silica glass: A possible indicator of subsurface fracture, Appl. Phys. Lett. (2012) 5.
[26] K. Sato, N. Kishimoto, K. Hirakuri, White luminescence from silica glass containing red/green/blue luminescent nanocrystalline silicon particles, J. Appl. Phys. (n.d.) 7.
[27] T. Calderon, A. Millan, F. Jaque, J.G. Solé, Optical properties of Sm^{2+} and Eu^{2+} in natural fluorite crystals, International Journal of Radiation Applications and Instrumentation. Part D. Nuclear Tracks and Radiation Measurements. 17 (1990) 557–561. https://doi.org/10.1016/1359-0189(90)90016-Q.

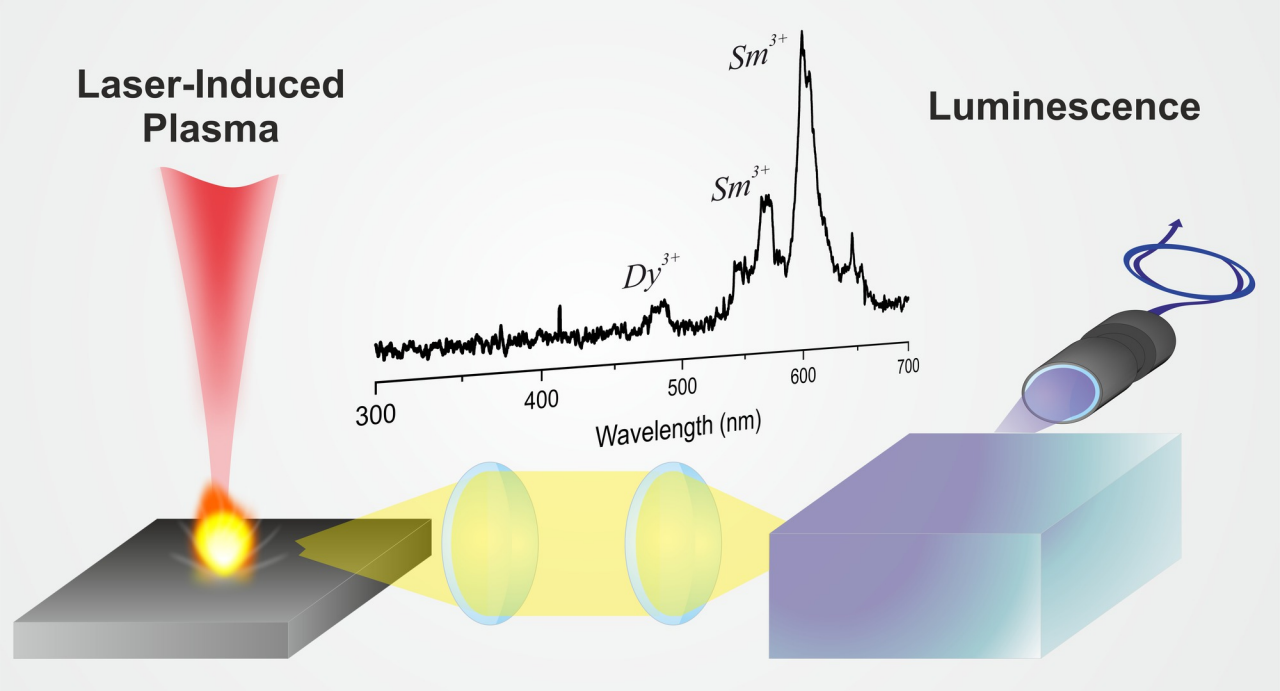
Laser-Induced Plasma
Luminescence
Sm^{3+}
Sm^{3+}
Dy^{3+}
300
400
500
600
700
Wavelength (nm)